

# Study of jetlike structure in high-transverse-energy events produced in $pp$ collisions at 400 GeV/ $c$

B. C. Brown, P. Devenski,\* H. Haggerty, and E. Malamud  
*Fermilab, Batavia, Illinois 60510*

R. Abrams, H. Goldberg, C. Halliwell, F. Lopez,† D. McLeod, and J. Solomon  
*University of Illinois at Chicago, Chicago, Illinois 60680*

A. Dzierba, J. Florian, R. Heinz, J. Krider, H. Martin, P. Smith, S. Teige, and A. Zieminski‡  
*Indiana University, Bloomington, Indiana 47405*

R. Ellsworth,§ R. Glasser, R. Holmes, P. Rapp, and G. Yodh  
*University of Maryland, College Park, Maryland 20742*

S. Ahn and T. Watts  
*Rutgers University, New Brunswick, New Jersey 08903*  
 (Received 28 November 1983)

The properties of events produced with high values of transverse energy in 400-GeV/ $c$   $pp$  collisions are presented. The events were collected using the large-acceptance Fermilab multiparticle spectrometer. The fraction of events that are planar when a full-azimuthal-acceptance trigger is used does not increase with transverse energy. However, when additional requirements are applied to the data such as restricting the azimuth or polar-angle acceptance, limiting the particle multiplicity, or requiring dominance of electromagnetic or hadronic energy within an event, the fraction of planar events increases with transverse energy. None of these requirements explicitly impose planar structure and we conclude that the data show an indication for the emergence of jetlike structure. The trend of the data is consistent with the predictions of a QCD model; it cannot be described by an extrapolation of uncorrelated low- $p_t$  phenomena.

## I. INTRODUCTION

We present in this paper results from Fermilab experiment E557, which studied the production of high-transverse-energy events in  $pp$  collisions at an incident momentum of 400 GeV/ $c$ . The goal of the experiment was to study production of jets in hadron-hadron interactions by employing a trigger that required a large amount of transverse energy ( $E_t \approx \sum |p_t|$  for relativistic particles) to be deposited in a calorimeter with full azimuthal acceptance and large polar-angle coverage. In our previous publication<sup>1</sup> we showed that such a trigger selects events that do not exhibit clear jet structure. Our results, which confirmed earlier observations of de Marzo *et al.*,<sup>2</sup> were recently supported by results from two other large-acceptance experiments<sup>3,4</sup> performed in the same energy range. Experiments at the CERN ISR<sup>4,5</sup> and at the CERN SPS collider<sup>6,7</sup> have established unambiguously copious production of jets in hadronic collisions at center-of-mass energies  $\sqrt{s}$  above 40 GeV. This suggests that large-acceptance triggers, which adequately select jets at large  $\sqrt{s}$ , must at lower energies be complemented by additional constraints imposed on the data.

It is of interest to extend the energy range of jet studies to lower energies to understand how competing mechanisms obscure the jet signal when large-acceptance triggers are used. With these aims in mind, we have analyzed our data using relatively unbiased methods to

select jet signals at lower energies.

The paper is organized as follows. Details of the apparatus and the triggers that were used are given in Sec. II. The analysis of the calorimeter response is discussed in Sec. III. In Sec. IV, we present yields as a function of  $E_t$  for various triggers. General properties of the data are discussed in Sec. V. In Sec. VI, we describe the search for jetlike structures in the data and discuss possible explanations for the failure of the large-acceptance trigger to select jets and present results of analyses of events selected by various hardware triggers and software cuts. In Sec. VII, we discuss the properties of the jetlike events selected in the previous section. Our conclusions are presented in Sec. VIII.

Throughout this paper an emphasis will be put on new experimental results. However, to illustrate the trends observed in the data we will occasionally compare the data with the predictions of two different models: a longitudinal-phase-space (LPS) model and a QCD gluon-bremsstrahlung model.<sup>8</sup> The comparisons will enable us to estimate the effects of energy-momentum conservation in large multiplicity events (comparison with the LPS model) and to search for jetlike structures in the data (comparison with the QCD model). We will limit model comparison to the event structure only because of the large uncertainties, both experimental and theoretical, in the absolute normalization of cross sections. The models are described in Sec. VI.

## II. APPARATUS

The experimental procedure as well as details of the apparatus have already been described in our previous publications.<sup>1,9</sup> We describe here the main features of the experiment relevant to the present analysis.

The layout of the apparatus is shown in Fig. 1. The experiment was performed using 400-GeV diffractively produced protons in the M6W beam line at Fermilab. The apparatus consisted of the Fermilab multiparticle spectrometer.<sup>10</sup> A typical beam intensity of  $0.5 \times 10^6$  protons was spread over a 1.0-s spill, which occurred once every 10 sec. The beam was incident on a 45-cm  $H_2$  target followed downstream by two interchangeable metal foils of Al, Cu, or Pb (Ref. 9) sufficiently thin that rescattering effects were negligible. Multiwire proportional chambers (34 planes of 8500 wires) and magnetostrictive spark chambers (24 planes) detected charged particles. Particle momenta were measured using a spectrometer magnet that provided a 0.2-GeV/ $c$   $p_t$  kick. Downstream of the tracking chambers was placed a  $2.3 \times 3.1$ -m<sup>2</sup> highly segmented calorimeter<sup>11</sup> consisting of 280 modules arranged into three sections (see Fig. 1). The upstream section, which consisted of 126 lead-scintillator sandwiches (16 radiation lengths  $L_r$ , and 0.8 absorption length  $L_a$ ), primarily measured the energy of electrons and photons (see Fig. 2). This electromagnetic section was followed by two hadronic sections of 126 and 28 iron-scintillator sandwiches, respectively ( $63L_r$  and  $7.5L_a$  combined). The distance from the center of the hydrogen target to the front face of the calorimeter was 9.4 m. The energy resolution of the calorimeter was measured to be  $\sigma/E = 0.2/\sqrt{E}$  for electrons and  $\sigma/E = 0.7/\sqrt{E}$  for hadrons, where the energy  $E$  is measured in GeV.<sup>11</sup> The calorimeter served both as a trigger (see below) and as a detector of neutral and charged particles (see Sec. III).

The geometrical acceptance of the apparatus was complete in azimuth for the polar-angle range  $59^\circ < \theta^* < 114^\circ$  as measured in the proton-proton center-of-mass frame [Fig. 2(a)]. The overall acceptance was estimated to be equivalent to  $2\pi$  azimuthal acceptance for  $47^\circ < \theta^* < 125^\circ$ . This corresponds approximately to a c.m. rapidity range  $0.65 < y^* < 0.84$ .

The apparatus was triggered in several ways. First an inelastic collision was detected by one of two methods. An incident proton was required to miss a counter of  $1 \times 1$  in. squared (designated  $1 \times 1$  in Fig. 1) placed on the beam

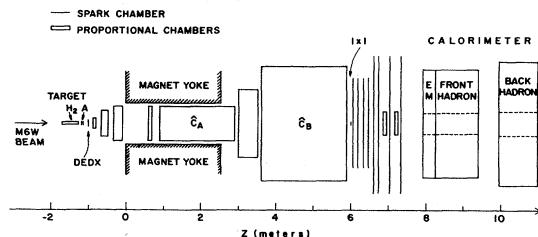


FIG. 1. The Fermilab multiparticle spectrometer.  $\hat{c}_A$  and  $\hat{c}_B$  are two multicelled Cherenkov counters whose outputs were not used in the analysis reported here.

line 7.5 m downstream of the target, or a large pulse height ( $\geq 2$  times minimum ionizing) was required to be registered in a counter (designated  $DE\ DX$  in Fig. 1) placed immediately downstream of the target. This constituted the “interacting-beam trigger” and was sensitive to approximately 90% of the total inelastic  $pp$  cross section. The other triggers consisted of this trigger with an additional requirement that at least a certain amount of transverse energy was present in some preset region of the calorimeter. For all the triggers the incident proton was required to be unaccompanied by another beam particle within  $\pm 130$  ns. Pulse-height information from a scintillation counter was used to eliminate rf buckets containing more than one particle. The rf buckets were 2 ns wide and were separated by 20 ns. A final veto on a following interaction occurring within  $\pm 200$  ns was imposed.

To form the calorimeter transverse-energy trigger the output from each module was weighted by the sine of the polar angle that the module subtended at the target.  $E_t$  sums for several different configurations of calorimeter modules were formed simultaneously. Data from three configurations are presented in this paper: full azimuthal acceptance (“global trigger”) and two limited  $\Delta\phi$  small aperture with approximate acceptance of 7.8, 165, and 0.70 sr, respectively, as measured in the proton-proton center-of-mass frame [see the shaded areas of Fig. 2(b)].

Data were collected with several  $E_t$  thresholds for each type of high- $E_t$  trigger. The absolute  $E_t$  scale from the calorimeter was determined by calibrating before and after the 18-day data run. In both cases a 20-GeV/ $c$  beam of electrons and hadrons was directed into each module. A 10% shift in the responses of individual modules typically occurred between the two calibrations. This shift was found to be consistent with the results of a laser monitoring system and with the observed time dependence of trigger rates. The variation of module responses was taken into account by assuming a linear dependence of the module gains with time between the two calibrations runs.

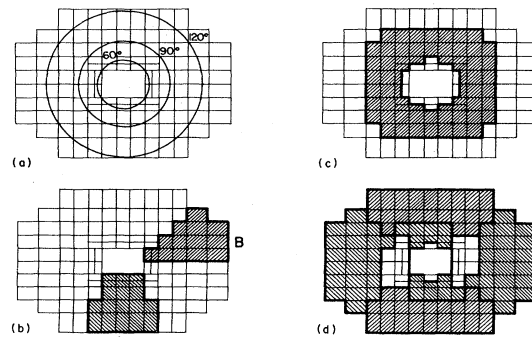


FIG. 2. A front-face schematic view of the electromagnetic and the upstream hadronic sections of the calorimeter. In (a) center-of-mass production angles for massless secondaries are shown; in (b) the two limited- $\Delta\phi$  apertures  $A$  and  $B$  used to form hardware triggers are shown; in (c) the modules used in the limited polar-angle-acceptance analysis are indicated; in (d) the module groups used in the modified “two-high” analysis (see text) are shown.

The response of the electromagnetic section of the calorimeter was found to be 17% larger for incident electrons than for hadrons. This effect was included by organizing module responses into electromagnetic and hadronic energy clusters (see next section).

In this analysis the spectrometer was used only to determine the position of the interaction vertex. The vertex resolution was  $\sigma=4$  mm as measured along the incident beam direction. This provided a clean hydrogen—nuclear-target separation.<sup>9</sup> The  $E_t$  sums for a given event were recalculated using the exact vertex position. A Monte Carlo simulation, based on the observed spectra of particles, was employed to unfold the energy resolution, energy leakage, and granularity of the calorimeter and to correct for the effects of the magnetic field. The total uncertainty of the  $E_t$  scale from the calibration and these sources was estimated to be  $\sigma(E_t)/E_t = \pm 5\%$ .

The  $pp$  interactions used in this analysis consisted of  $(32, 16, \text{ and } 6) \times 10^3$  events taken with the interacting-beam, global, and limited  $\Delta\phi$  triggers, respectively. They were selected by requiring an interaction vertex to be within the 40-cm long fiducial volume of the  $H_2$  target. In addition, the observed  $E_t$  was required to exceed the hardware threshold by at least 1-GeV transverse energy. The integrated luminosity for the global and limited  $\Delta\phi$  trigger data sets was 4 and  $2 \text{ nb}^{-1}$ , respectively.

### III. ANALYSIS

Much of the analysis presented in this paper was performed using the calorimeter module outputs directly. This was appropriate for studying yields and general event structure. To perform more detailed studies (e.g., multiplicity of secondaries, jet reconstruction, etc.) it was necessary to organize the responses of the calorimeter modules into energy clusters henceforth known as “calorimeter tracks.” The cluster forming algorithm first combined the responses of corresponding electromagnetic and hadronic modules to form responses of “dual modules.” The dual module with the largest response was then found. This dual module, together with all adjacent dual modules, formed a group whose responses contributed to the energy of a cluster. Energy was assigned to a cluster by comparing the actual energy deposition within the group with the predictions of a shower simulation.<sup>12</sup> The center of a shower (cluster) was obtained by averaging the positions of the clusters of dual modules within the group weighted by the squares of their responses. The cluster was designated to be electromagnetic or hadronic depending on its energy deposition pattern in the electromagnetic and hadronic calorimeters. Modules whose responses were badly inconsistent with the predictions of the shower simulation were removed from the group and a new prediction was made. The difference between the actual module responses and the predictions from the shower simulation was then calculated and the procedure was repeated for the next remaining dual module with the highest energy. This procedure was repeated until clusters with energy less than 1 GeV remained; these were ignored. The effects of the systematic errors due to the cluster-finding algorithm are discussed in Sec. V.

We have found the multiplicity of electromagnetic tracks so formed to be greater than half of the hadronic multiplicity. Electromagnetic tracks presumably contain a mixture of resolved photons and unresolved neutral pions and hence are unsuitable for calculating  $\pi^0$  and  $\eta^0$  multiplicities. Therefore we do not compare production rates for electromagnetic tracks with the known  $\pi^0$  and  $\eta^0$  inclusive cross sections; we will concentrate instead on the comparison of hadronic track-production rates.

Hadronic tracks consist mainly of charged pions with a few-percent addition of charged and neutral kaons. In Fig. 3, we compare the  $E_t$  spectrum of hadronic calorimeter tracks detected between  $60^\circ$  and  $120^\circ$  as measured in the center-of-mass frame with relevant inclusive cross sections measured in other experiments.<sup>13,14</sup> The hadronic track data agree to within 20% with published cross sections over a wide  $p_t$  range ( $0.5 < p_t < 5 \text{ GeV}/c$ ). This agreement gives us confidence in the performance of our cluster finding algorithm and in the calibrated  $E_t$  scale of the experiment. In Fig. 4, we compare multiplicity distributions of the hadronic tracks with charged-particle data obtained in another  $pp$  experiment using a similar center-of-mass energy and an apparatus with a similar rapidity acceptance.<sup>15</sup> The difference between Ref. 15 data and E557's data could be greatly reduced if corrections were made for Ref. 15's incomplete azimuthal acceptance (90% of  $2\pi$ ) and the detection of neutrons and  $K_L^0$ 's in E557's

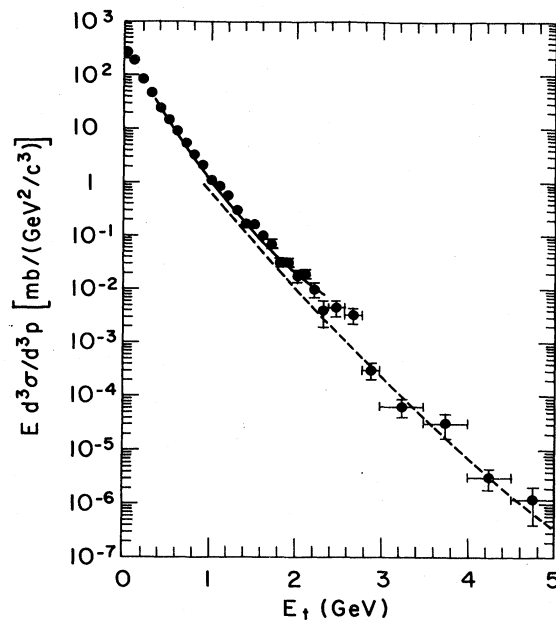


FIG. 3. Invariant differential cross sections for the production of hadronic clusters in the pseudorapidity range  $2.82 < \eta_{\text{lab}} < 3.92$ . Only statistical errors are shown; systematic errors are estimated to change the results by approximately  $\pm 20\%$  for  $E_t$  values greater than 2.5 GeV. The solid curve is the result of parametrizing the world data for the single-particle production of  $\pi^\pm$ ,  $K^\pm$ ,  $p$ , and  $\bar{p}$ 's (Ref. 13). The dashed curve is a fit to single-charged-particle data (the sum of  $\pi^\pm$ ,  $K^\pm$ ,  $p$ , and  $\bar{p}$ ) measured at  $90^\circ$  in the center-of-mass (Ref. 14). The world-data parametrization did not include the data from Ref. 14.

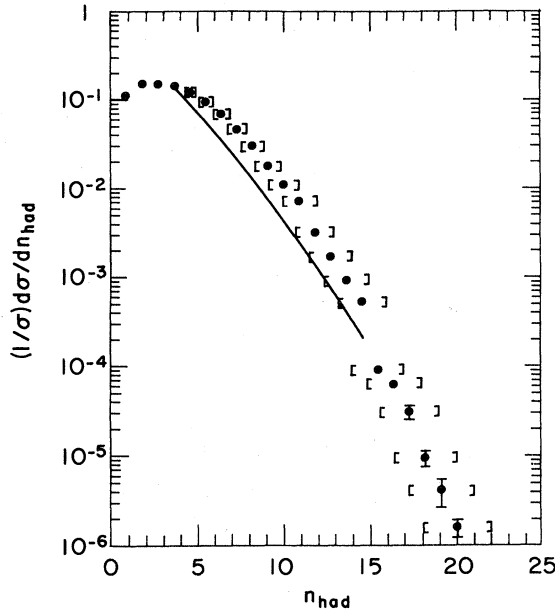


FIG. 4. Hadronic-cluster multiplicity distribution. Statistical errors (vertical lines) and systematic uncertainties (horizontal brackets) are both shown. The curve is a fit to the data reported in Ref. 15.

calorimeter. We conclude that typical hadronic multiplicities (of, say, 15) are known to  $\pm 2$ . We also note that there is no indication of substantial merging of hadronic tracks in large multiplicity events.

Even though electromagnetic tracks did not correspond to single photons, they were still used extensively to form variables that were not sensitive to this fact (e.g., the formation of total  $E_t$ ).

#### IV. YIELDS

It has been previously shown that  $E_t$  yields vary strongly with the acceptance of the apparatus.<sup>1,2</sup> For those studies a large range of acceptances was used ( $7.8 > \theta^* > 0.7$  sr). In order to see if this trend still exists when a small range of acceptances are used, the yields from the two limited  $\Delta\phi$  calorimeter sectors [denoted A and B in Fig. 2(b)] are compared in Fig. 5. An increase of a factor of 2.3 in acceptance causes a change of approximately 10 in yield. This is an indication that the secondaries hitting the calorimeter within the trigger acceptance are distributed throughout the entire aperture of the triggering sector and little collimation of secondaries is occurring within it. There is also no indication of the yields exhibiting a power-law dependence on  $E_t$ . Such a variation would be expected if a hard-scattering process was dominating the production mechanism.

Yields for small acceptances were obtained by an alternative method using solely the data obtained when the global trigger was used. For each event the  $E_t$  within the geometrical areas of sectors A and B was calculated off line. Since the data were collected using various global  $E_t$  thresholds, the number of events within a given  $E_t$  bin,

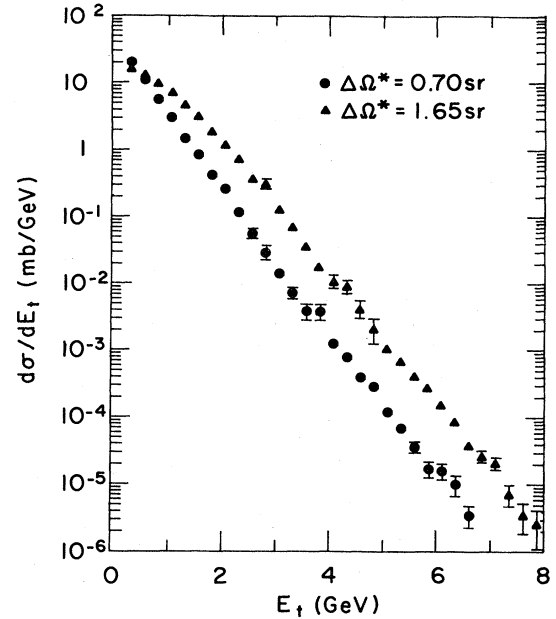


FIG. 5. Yields detected in sectors A (triangles,  $\Delta\Omega^* = 1.65$  sr) and B (circles,  $\Delta\Omega^* = 0.70$  sr) of the calorimeter as a function of transverse energy in the respective sectors. Statistical errors only are shown. The uncertainty in the  $E_t$  scale is estimated to be  $\pm 5\%$ .

$dN/dE_t$ , did not correspond to the measured cross section  $d\sigma/dE_t$ . In order to restore this correspondence events were given appropriate weights,  $w = (d\sigma/dE_t) / (dn/dE_t)$ . We have found the yields obtained by this analysis agree to within a factor of  $\sim 2$ . The difference is due to methods used to correct the raw data and represents the systematic error in the measured cross section. We note that present theoretical predictions for the high- $E_t$  rates are also subject to similar or even larger uncertainties. Consequently, our global data can be used with software cuts to simulate reduced-aperture triggers.

In an attempt to decrease systematic errors due to energy leakage out of sectors A and B and to facilitate comparison with theoretical predictions, we have used the global data to produce cross sections in well defined  $\theta^*$  and  $\phi$  regions. The  $\theta^*$  acceptance (assuming massless secondaries) was restricted to the range  $120^\circ > \theta^* > 60^\circ$  as shown in Fig. 2(a).

The chosen polar-angle range had the advantage that it allowed one to perform symmetry checks on the data. Two pie-shaped back-to-back sectors were formed with each sector subtending  $\Delta\phi = 45^\circ$  in azimuth. The sectors were situated in the up-down and left-right configurations as viewed along the incident beam direction. A comparison of yields showed a difference of a factor of 2 for the two configurations (this was after magnetic-field kick corrections). In addition, yields from the polar-angle region  $60^\circ < \theta^* < 90^\circ$  were compared with those from  $90^\circ < \theta^* < 120^\circ$ . They agreed to within a factor of 2 also. We conclude, as before, that yields can be trusted typically to a factor of 2.

Yields from various-sized pie-shaped sectors are plotted in Fig. 6. The characteristics seen previously from large-acceptance hardware-triggered sectors are plainly visible: the increasing dependence on  $E_t$  with decreasing acceptance and the strong dependence on aperture size. One can also see that no deviation from an exponential variation occurs at high values of  $E_t$ , even for small ( $\Delta\phi = 11.25^\circ$ ) sized sectors.

### V. GENERAL PROPERTIES OF EVENTS

In this section we describe general properties of events obtained using the global trigger and discuss their dependence on  $E_t$ .

The transverse energies of individual tracks were summed to form total electromagnetic and hadronic transverse energies separately. The ratio of these two types of transverse energies decreased from 0.8 for  $E_t < 4$  GeV values ( $E_t$  is the sum of the two types of transverse energy) to 0.35–0.45 at  $E_t = 10$  GeV; above 10 GeV it remained constant. The relative importance of electromagnetic energy at large angles for low- $E_t$  events is qualitatively predicted by the longitudinal-phase-space (LPS) model. Also the observed value of the electromagnetic to hadronic  $E_t$  ratio at high- $E_t$  values is in a reasonable agreement with the model predictions. However, the

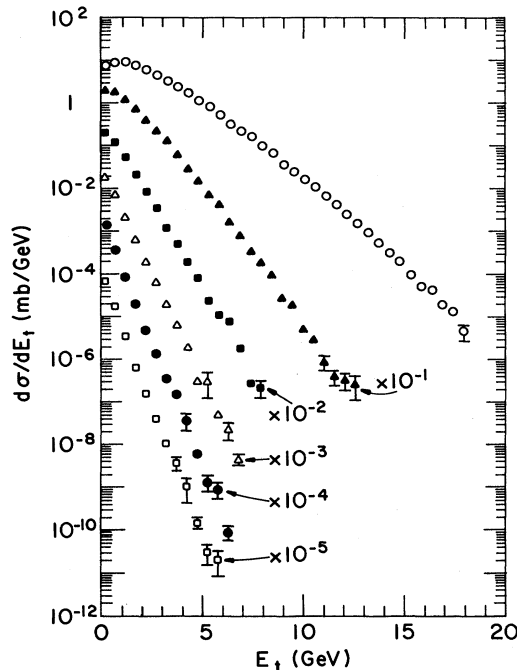


FIG. 6. Yields obtained by applying a software acceptance cut of  $2.82 < \eta_{\text{lab}} < 3.92$  to the global data. The circles, full triangles, full squares, open triangles, dots, and open squares refer to data obtained with  $2\pi$ ,  $\pi$ ,  $\pi/2$ ,  $\pi/4$ ,  $\pi/8$ , and  $\pi/16$  azimuthal acceptances, respectively. For reasons of clarity, the results from the  $\pi$ ,  $\pi/2$ ,  $\pi/4$ ,  $\pi/8$ , and  $\pi/16$  acceptances have been multiplied by  $10^{-1}$ ,  $10^{-2}$ ,  $10^{-3}$ ,  $10^{-4}$ , and  $10^{-5}$ , respectively. Only statistical errors are shown. The uncertainty in the  $E_t$  scale is estimated to be  $\pm 5\%$ .

experimental value of the ratio is subject to a large systematic error due to uncertainties of the cluster-forming algorithm; specifically, two calorimeter tracks, one hadronic, one electromagnetic could be formed occasionally when only a single hadronic track really existed. To estimate the systematic error due to this we have forcibly merged closely spaced tracks. The result was that the ratio dropped by 0.10. We consider this change to represent a systematic error for the discussed ratio. We note that such a systematic error has a small effect on hadronic multiplicities and causes the average transverse energy of a hadronic track to be changed by 100 MeV.

In Fig. 7, we show the variation of average hadronic calorimeter track multiplicity detected in the calorimeter with total transverse energy and compare it with the predictions of the LPS and QCD models. No  $E_t$  cut (other than their energy being greater than 1 GeV) and no acceptance cuts have been applied to the calorimeter tracks. As expected, an increase in multiplicity with total  $E_t$  occurs. The rate of increase appears to lessen as  $E_t$  is increased; this is reminiscent of an effect reported previously.<sup>2</sup> One can see that the predictions of both models are in good agreement with data in the range  $E_t < 11$  GeV. Above 11 GeV the LPS model predicts a larger multiplicity than the data. This is a direct consequence of limiting the transverse momenta of the secondaries in the model.

Even though there is an increase in hadronic multiplicity with  $E_t$ , it is not strong enough to maintain the ratio of transverse energy to hadronic cluster multiplicity at a constant value. This is shown in Fig. 8. The average ratio approaches 0.7 GeV/c for events with total transverse en-

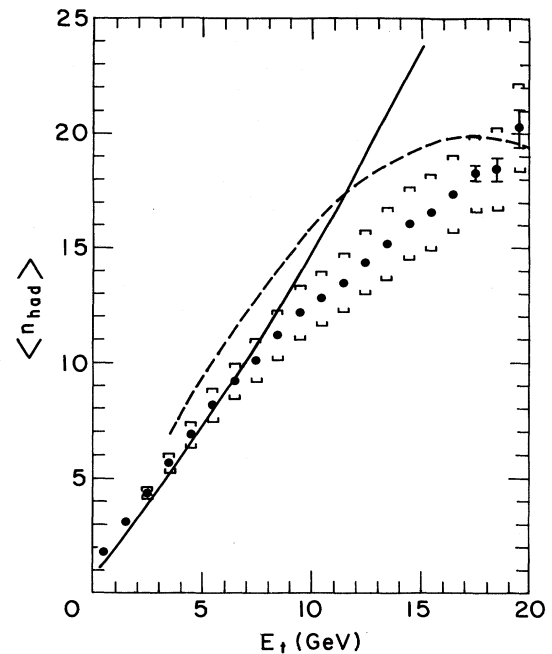


FIG. 7. The average hadronic-cluster multiplicity detected in the calorimeter. The solid and dashed curves are the predictions of the LPS and QCD models, respectively. Statistical errors (vertical lines) and systematic uncertainties (vertical parentheses) are both shown.

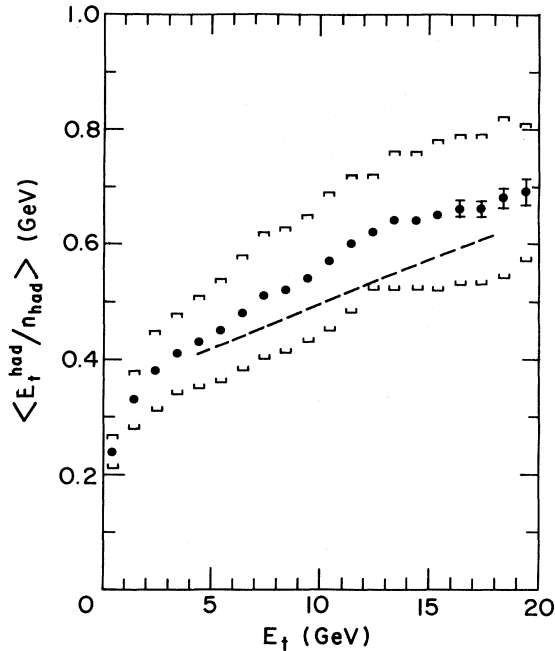


FIG. 8. The dependence of the average transverse energy of hadronic clusters on the total transverse energy detected in the calorimeter. Statistical errors (vertical lines) and systematic uncertainties (vertical brackets) are both shown. The dashed curve is the predictions of the QCD model.

ergy, in agreement with that reported at 300 GeV for  $pp$  and  $\pi^-p$  interactions [ $\sim 0.65$  GeV (Ref. 2)]. From Fig. 8 one can see that the QCD model predicts the increase of this ratio with  $E_t$ .

From Figs. 7 and 8, we conclude that high-transverse-energy events typically have a large number of secondaries with each particle individually having a relatively small amount of transverse momentum.

Event structure was studied in more detail in terms of the planarity variable,<sup>1,2</sup> which was calculated in the transverse plane of the event. In this projection an event axis was chosen arbitrarily and the  $p_t$  vector for each calorimeter track was decomposed into components parallel and transverse to this axis. Denoting the sums of the squared components along and transverse to the event axis as  $A$  and  $B$ , then planarity is defined as  $P = (A - B) / (A + B)$ .  $P$  was then maximized by varying the direction of event axis. For pencil-like back-to-back jets,  $P$  approaches 1, while for isotropic events with large multiplicity it approaches 0. Figures 9(a) and 9(b) show the observed planarity distributions for events with  $7 < E_t < 14$  GeV and  $E_t > 14$  GeV, respectively, for the global data sample (similar distributions were obtained directly from using calorimeter module responses). It is clear that the majority of the events are nonplanar. This is summarized in Fig. 10(a), where the average planarity as a function of  $E_t$  is shown. In addition, the fraction of high-planarity events ( $P > 0.7$ ) with high values of  $E_t$  is equal to 9% and remains constant. This is shown in Fig. 10(b).

In order to see whether the high-planarity events are

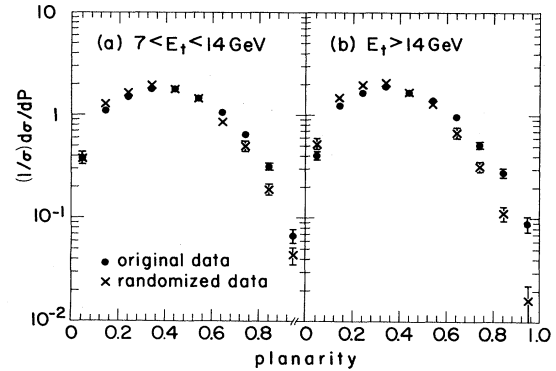


FIG. 9. Planarity distributions for events with (a) medium values of transverse energy ( $14 > E_t > 7$  GeV) and (b) high values of transverse energy ( $E_t > 14$  GeV). The original data (circles) and randomized data (crosses) are both shown.

primarily due to fluctuations of typical events we used the experimental data themselves rather than the predictions of the LPS model since the simulation of these rare events would depend heavily on the specific input parameters of the model. Using the experimental data overcomes this

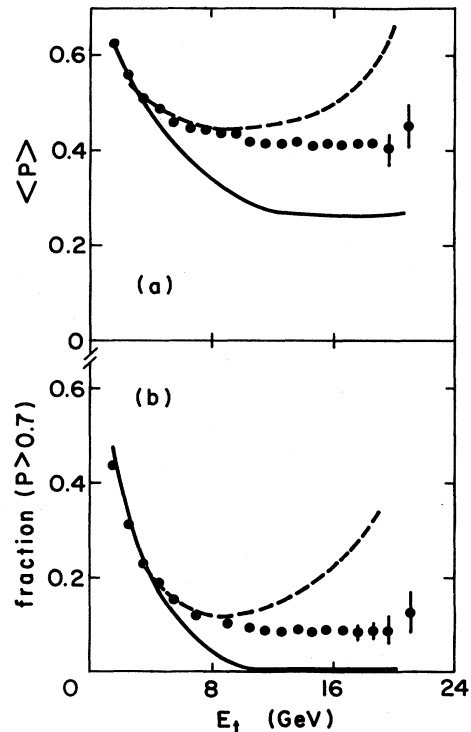


FIG. 10. (a) Average planarity (calculated using the global data) as a function of transverse energy detected in the total calorimeter. The solid and dashed curves are the predictions of the LPS and QCD models, respectively. (b) The fraction of events in the global data set that possess planarity values greater than 0.7 as a function of transverse energy detected in the total calorimeter. The solid and dashed lines are the predictions of the LPS and QCD models, respectively.

objection. We randomized the directions of all of the calorimeter tracks independently in the transverse plane (their polar directions were preserved). Consequently, any spatial correlations between particles were destroyed. The randomization procedure was repeated until the magnitude of the original  $p_t$  imbalance measured in the calorimeter was reproduced to within  $\pm 2\%$  (the results did not change significantly when this requirement was relaxed to  $\pm 25\%$ ). Planarity was then recalculated using the randomized calorimeter tracks. By performing this randomization we aim to study how the event structure is constrained from energy-momentum conservation alone.

The effect of this analysis is shown in Fig. 11, where the transverse-energy flow for events with  $E_t > 14$  GeV is plotted. The original data are compared to the randomized tracks. Even though two small excesses exist, one near the track with maximum transverse energy ( $\phi = 0^\circ$ ) and one opposite to it ( $\phi = 180^\circ$ ), from the sizes of the excesses we conclude that the structure of a typical high- $E_t$  event is governed primarily by energy-momentum conservation.

However, from Figs. 9(a) and 9(b), one can see that a deficit of *high-planarity* randomized events is produced indicating that high-planarity events are *not* totally caused by statistical fluctuations of low-planarity ones. The excess of original high-planarity events above those produced by the randomization procedure increases strongly with total  $E_t$ . This is shown in Fig. 12. This increase is in contrast to the constancy of the fraction of original high-planarity events shown in Fig. 10(b). We conclude from Fig. 12 that approximately 40% of events with  $E_t > 14$  GeV and  $P > 0.7$  are caused by dynamical effects other than statistical fluctuations of large-multiplicity low- $p_t$  events.

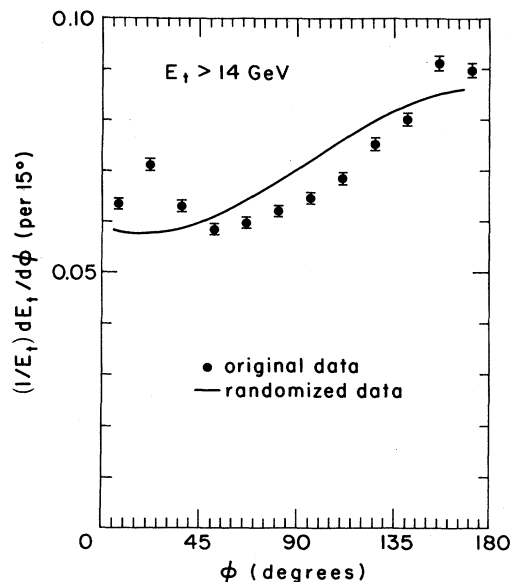


FIG. 11. Transverse-energy flow as a function of azimuthal angle as measured from the track with maximum transverse energy. The original data (points) and a fit to the randomized data (solid curve) are shown. The transverse energy of the maximum  $E_t$  track is not included in this plot.

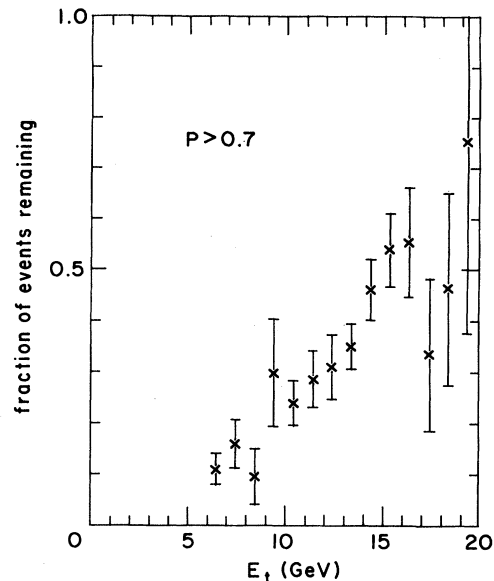


FIG. 12. The fraction of events with  $P > 0.7$  that remain with  $P > 0.7$  after randomization. Statistical errors only are shown.

## VI. SEARCH FOR JETLIKE STRUCTURES

In order to search for jetlike structures within the global and limited  $\Delta\phi$  data sets we performed several cuts. It is apparent from arguments presented in the previous section that one of the most fundamental would be  $E_t$  requirement. This view is supported by the theoretical work of Akesson and Bengtsson,<sup>16</sup> who have made a quantitative prediction for the minimum value of  $E_t$  above which hard scattering should become the dominant process for a given aperture. According to these authors the crossover value of  $E_t$  is equal to

$$E_t^{\text{CO}} = 16 \Delta y (\Delta\phi/2\pi) \text{ GeV},$$

where  $\Delta y$  is the rapidity interval and  $\Delta\phi$  the azimuthal-angle interval included in the trigger (the value of  $E_t^{\text{CO}}$  is, to first approximation, independent of the c.m.-energy squared of the colliding particles). For this experiment one would not expect to see jets dominating the global data for events with the values of  $E_t$  below 24 GeV. This is not in disagreement with the jet signal presented in the previous section which constituted only 5% of *total* data with  $E_t > 14$  GeV. For the limited  $\Delta\theta^*$  acceptance data one would expect jets to dominate above 15 GeV.

Several theoretical models offer explanations for the lack of jet dominance in the events selected with a global trigger.<sup>8,16-20</sup> Processes that might obscure the jet signal essentially fall into three categories: (i) contribution to the measured transverse energy from fragments of spectator jets,<sup>17,18</sup> (ii) gluon bremsstrahlung before and after the hard scatter,<sup>8,18,19</sup> and (iii) two competing processes: a large-multiplicity tail of low- $p_t$  type collisions and hard scatters with the relative contribution of the two processes depending on the aperture of the calorimeter trigger.<sup>16,20</sup> The results from several previous experiments suggest

suitable cuts on the data. For example, a large-aperture experiment at the ISR<sup>5</sup> has reported the emergence of jets when triggered on the electromagnetic component of transverse energy alone. A Fermilab experiment<sup>21</sup> combined a requirement of large global  $E_t$  with restricted multiplicity or with the presence of two or more energetic clusters<sup>3,22</sup> (so called “two-high” triggers<sup>3</sup>).

In order to select jetlike events from the background of competing processes we studied events selected by hardware and software triggers with (A) limited aperture in the azimuth, (B) limited aperture in the polar angle, (C) a modified two-high trigger requirement, (D) limited particle multiplicity in the final state, (E) electromagnetic or hadronic  $E_t$  dominating the global  $E_t$ , and (F) a transverse-energy cut on the secondaries.

The data presented in this section are compared with predictions of the LPS and QCD models.

The LPS model takes into account the leading-nucleon effect and correctly reproduces multiplicities and  $p_t$  spectra of particles as known from bubble-chamber experiments.<sup>23</sup> It also includes a long tail of large multiplicities in the multiplicity distribution which for  $n_{ch} > 28$  is generated according to an exponential form  $\exp(-3n_{ch}/\langle n_{ch} \rangle)$ , where  $n_{ch}$  and  $\langle n_{ch} \rangle$  are the charged-particle multiplicity and the average value, respectively. In this model particles are produced in an uncorrelated fashion except for strict energy-momentum conservation which is imposed for each generated event. The model does have its limitations; it predicts an average transverse momentum for the secondaries which does not vary with event  $E_t$ . This is in disagreement with the data (see Fig. 8). Therefore we will use this model with caution; it will be primarily used to estimate the effects of energy-momentum conservation.

The QCD model represents an upgraded version of the four-jet model.<sup>24</sup> It takes into account gluon bremsstrahlung from the initial and scattered partons. The final-state quarks (gluons decay into  $q\bar{q}$  pairs) are organized into colorless pairs and fragmented into hadrons according to either the Field-Feynman scheme<sup>25</sup> or phase space depending on the invariant mass of the pair. The spectator quarks from the initial hadrons are treated in the model as single partons.

In our calculations we have used standard values of parameters as suggested by the authors of Ref. 8, except for the after-scatter beam cutoff  $t_A^{\min}$ , whose value has been changed from 3 to 1 (GeV/c)<sup>2</sup>. Only hard scatters with  $p_t > 1.5$  GeV/c were considered. However, most of the model predictions for event structure are insensitive to this cutoff. The parameters of the models have been taken from the literature and have not been “tuned” to optimize agreement with our data.

#### A. The limited- $\Delta\phi$ -aperture data

For this analysis we have selected data triggered by a deposition of  $E_t$  in sector A of the calorimeter [see Fig. 2(b)].

The average planarity  $\langle P \rangle$  calculated using module responses from the entire calorimeter, increases monotonically with the transverse energy detected in the triggering

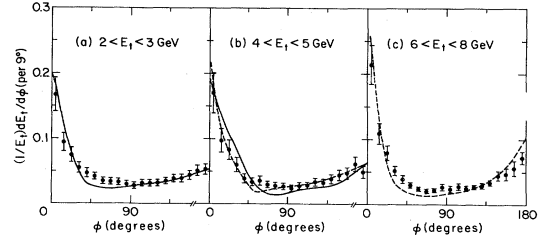


FIG. 13. Average planarity as a function of  $E_t$  for events obtained using a limited  $\Delta\phi$  trigger. Planarity was calculated using the responses from all modules;  $E_t$  was formed using the responses from triggering modules alone. The solid and dotted curves are the predictions of the LPS and QCD models, respectively.

sector (Fig. 13), indicating that events become more jetlike with increasing  $E_t$ . This increase is mainly due to the collimation of particles within the triggering sector. The increase for  $E_t$  values above 4 GeV is predicted by the QCD model whereas the LPS model predicts the rise at low  $E_t$ .

The transverse-energy flow as measured by the whole calorimeter is plotted in Fig. 14 as a function of azimuthal angle ( $\phi=0$  is defined as the center of the triggering sector). The low- $E_t$  data agree well with predictions of the LPS model. For data with medium  $E_t$  ( $4 < E_t < 5$  GeV) both the LPS and QCD models predict the general trends of the data; the QCD model is in better agreement

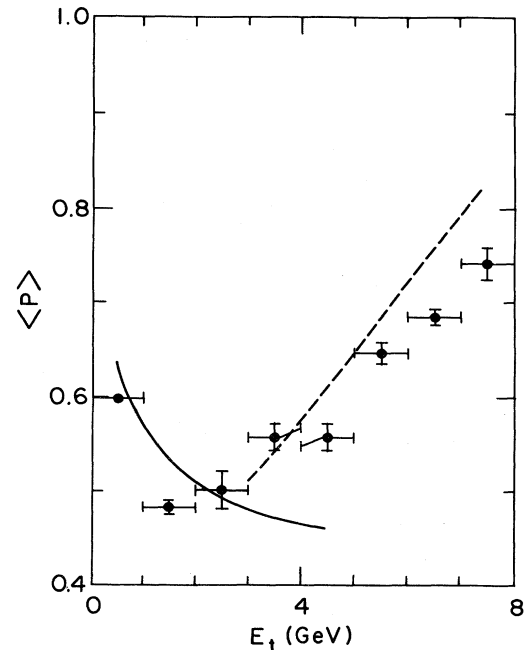


FIG. 14. Normalized transverse-energy flow vs azimuthal angle as measured from the center of the triggering sector. Low- ( $2 < E_t < 3$  GeV), medium- ( $4 < E_t < 5$  GeV) and high- $E_t$  ( $6 < E_t < 8$  GeV) data sets are shown.  $E_t$  is the transverse energy detected in the triggering sector alone. The solid and dashed curves are predictions of the LPS and QCD models, respectively.



with measured energy flow within the triggering sector ( $\Delta\phi=0^\circ$  to  $30^\circ$ ). This is seen to be so also for the high- $E_t$  data.

To study in greater detail the collimation effect within the triggering sector we follow Ref. 26 and introduce the variable pseud thrust  $T$ , defined as

$$T = \frac{\sum_i |\hat{e} \cdot \vec{p}_{ti}|}{\sum_i |\vec{p}_{ti}|},$$

where the sums are carried out over the modules in the triggering sector and  $\hat{e}$  is a unit vector along the direction of  $\sum_i \vec{p}_{ti}$ . The experimental size of the triggering sector limits the range of  $T$  to values from 0.85 (two maximally separated tracks) to 1 (pencil-like jets). The fraction of events with  $T > 0.96$  rises as a function of  $E_t$  (see Fig. 15). This is similar to the effect seen in Fig. 13 and once again the QCD model is successful in predicting the increased collimation at high values of  $E_t$ . The LPS model is unable to account for this effect because of the model's method of producing large values of  $E_t$ . It does so by producing a large number of low- $p_t$  secondaries randomly in azimuth.

We notice that a collimation effect on the trigger side ( $\phi=0^\circ$ ) does not lead to a detectable increase in collimation on the side opposite to the triggering sector ( $\phi=180^\circ$ ). Transverse-energy flows for low- and high- $T$  events are very similar (Fig. 16). Both energy flows agree well with QCD predictions.

Results for the limited- $\Delta\phi$  trigger presented here were obtained for events selected by a hardware trigger. We obtain similar distributions from a software-acceptance cut imposed on the global data. We conclude that the global data with software cuts can be used not only to derive cross sections for smaller apertures as shown in Sec. III,

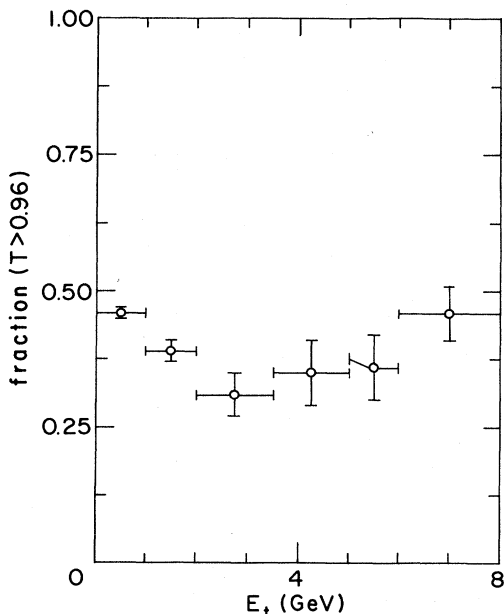


FIG. 15. The fraction of events without pseud thrust greater than 0.96 as a function of  $E_t$ .  $E_t$  is the transverse energy detected in the triggering sector.

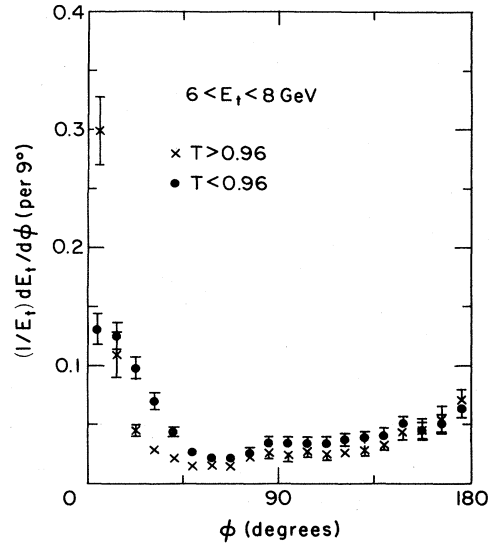


FIG. 16. Normalized transverse-energy flows for events with high and low pseud thrust values ( $T > 0.96$  and  $T < 0.96$ , respectively).  $\phi=0^\circ$  corresponds to the center of the triggering sector.

but also to study event structure in detail. This will be used extensively in the following analyses.

#### B. The limited- $\theta^*$ -aperture data

For this analysis we used exclusively the pulse-height information from the calorimeter modules. We have introduced software acceptance cuts on the global data. The global-trigger acceptance was reduced to approximately  $63^\circ < \theta^* < 110^\circ$  ( $\Delta\Omega^* = 5.0$  sr), as shown in Fig. 2(c).

The event structure does not change with  $E_t$  when no acceptance cuts are applied to the global data<sup>1</sup> (see Fig. 10). The "reduced" global data obtained by applying the above cut do, however, exhibit a statistically significant shift towards larger planarity values for  $E_t > 12$  GeV. This is shown in Fig. 17 where planarity distributions (using modules from the entire calorimeter) are shown as a function of  $E_t$  (calculated using modules from the limited acceptance alone). The increase in the number of high-planarity events is emphasized in Fig. 18 where the average planarity and the fraction of high-planarity events is shown as a function of  $E_t$  (calculated as before). A comparison with the LPS and QCD model predictions is also shown. As noted in the limited  $\Delta\phi$  analysis, the LPS model does not predict the increased collimation. In contrast to this the QCD model predicts a substantial increase in planarity at high values of  $E_t$ .

We note that the QCD model also predicts increasingly planar events for events detected using the full calorimeter acceptance (see Fig. 10). We conclude from a comparison of Figs. 10 and 18 that decreasing the polar acceptance of the calorimeter diminishes the nonjetlike event structure present in the experimental data. The source of this structure could be for example, beam and target fragments.

The increase of  $\langle P \rangle$  is also observed when  $\langle P \rangle$  is cal-

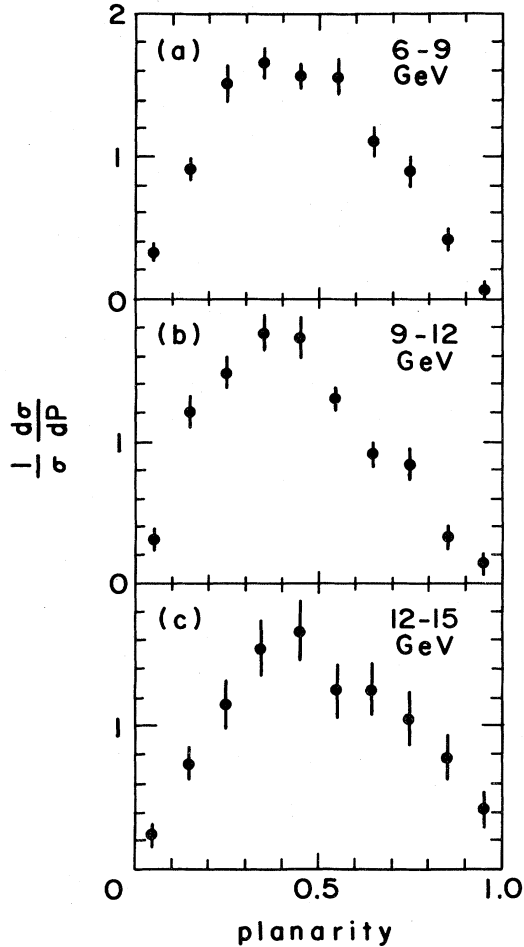


FIG. 17. Planarity distributions for the limited- $\theta^*$ -acceptance global data. The three  $E_t$  ranges (6 to 9, 9 to 12, and 12 to 15 GeV) were calculated using only the responses from the modules within a reduced  $\theta^*$  aperture.

culated using only those modules which are included in the restricted acceptance. Both effects are also present when calorimeter tracks rather than module responses are used. The increase in  $\langle P \rangle$  is therefore not due to effects such as granularity of the calorimeter.

### C. Modified two-high trigger

This analysis was based on software cuts imposed on the global data and it also used calorimeter module responses.

We have divided the calorimeter into eight regions [see Fig. 2(d)] each covering approximately  $\Delta\phi=90^\circ$  and  $\Delta\theta^*=35^\circ$  with  $\Delta\Omega^*$  ranging from 0.9 to 1.2 sr. In addition to demanding a high value of  $E_t$  in the entire calorimeter, we required the value of transverse energy in two of the eight groups to exceed a certain threshold  $E_t^{\text{thr}}$ . Since there was no constraint on the relative alignment of these two chosen groups, any of the 28 combinations of pairs may occur. Only eight of these combinations corre-

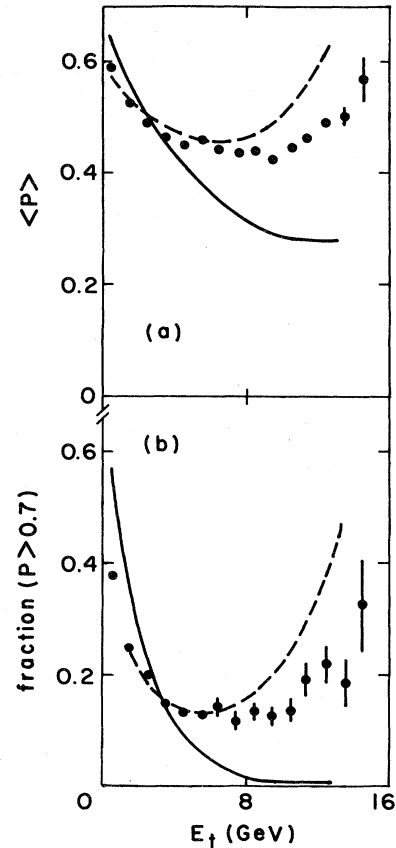


FIG. 18. (a) The average planarity of events and (b) the fraction of high-planarity events as a function of  $E_t$  calculated using the responses from the modules within a reduced  $\theta^*$  aperture. The solid and dashed curves are the predictions of the LPS and QCD models, respectively.

spond to kinematically favored “back-to-back” and “back-antiback” configurations in the  $\phi$  and  $\theta^*$  angles. In Fig. 19, we plot the fraction of global  $E_t$  triggers fulfilling the additional two high requirement as a function of  $E_t^{\text{thr}}$ . A 3-GeV cutoff selects only 5% of all events with  $E_t > 12$  GeV, 70% of which correspond to back-to-back or back-to-antiback configurations. The LPS model predicts this trend well indicating that such event structure is dominated by energy-momentum considerations rather than jet production. This is confirmed in Fig. 20 where the average planarity of events selected by this method increases with  $E_t^{\text{thr}}$ . We conclude that there is no overwhelming evidence that a two-high-type trigger unambiguously selects events caused by hard scattering.

### D. Limited particle multiplicity in the final state

For this analysis we used hadronic calorimeter tracks rather than module responses; no acceptance cuts were applied to the data. The multiplicity and planarity were determined for each event. Average planarity values for

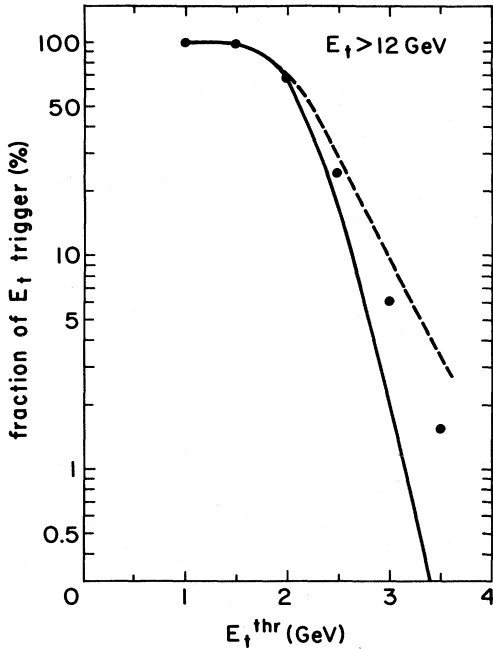


FIG. 19. Fraction of events with  $E_t > 12$  GeV and with two limited-acceptance regions both possessing  $E_t > E_t^{\text{thr}}$ . The solid and dashed curves are predictions of the LPS and QCD models, respectively.

low- and high-multiplicity events were then plotted (see Fig. 21). The increase in planarity for low-multiplicity events confirms a result reported earlier<sup>21,22</sup> using all calorimeter tracks, electromagnetic and hadronic. The difference between the mean planarities for low- and high-multiplicity events is partially due to the correlation between planarity and multiplicity and is at least qualitatively predicted by both the LPS and the QCD models.

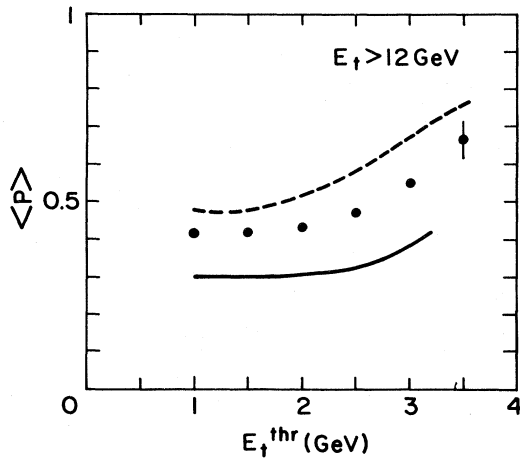


FIG. 20. Average planarity of events with  $E_t > 12$  GeV and with two limited-acceptance regions both possessing  $E_t > E_t^{\text{thr}}$ . The solid and dashed curves are predictions of the LPS and QCD models, respectively.

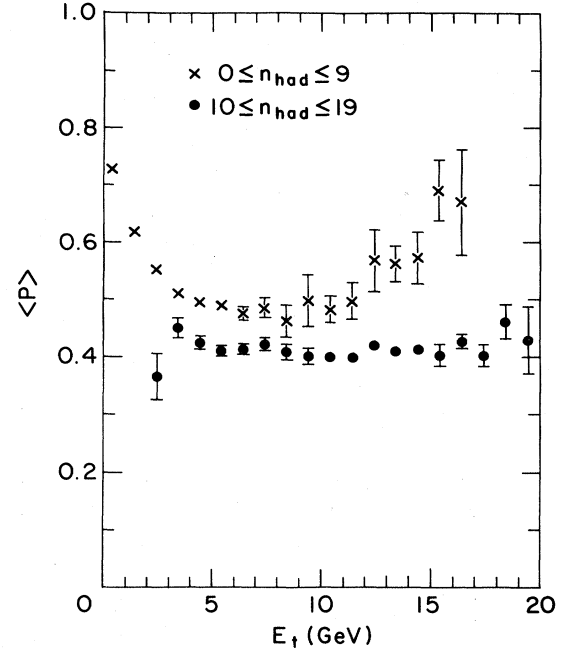


FIG. 21. Average planarity (calculated using all calorimeter tracks) for events with low and high hadronic track multiplicity.

Consequently, it is difficult to assess whether the increase at high  $E_t$  is due mainly to kinematic effects or has a deeper dynamic origin.

#### E. Electromagnetic and hadronic components of global $E_t$

In Sec. III, we described how a calorimeter track was designated to be electromagnetic (em) or hadronic (had). The transverse energies of the individual tracks were summed to form total electromagnetic and hadronic energies separately ( $E_t^{\text{em}}$  and  $E_t^{\text{had}}$ , respectively). The sum  $E_t^{\text{em}} + E_t^{\text{had}}$  was equal to the total transverse energy in the event,  $E_t$ .

In Fig. 22(a) we show the dependence of average planar-

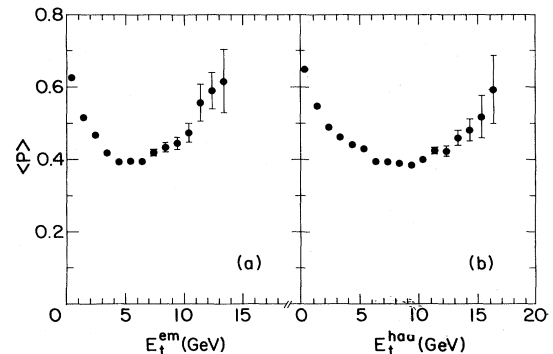


FIG. 22. Average planarity (calculated using all calorimeter tracks) as a function of the total (a) electromagnetic and (b) hadronic transverse energy detected in the calorimeter. Only statistical errors are shown.

ity (calculated using *all* tracks) as a function of  $E_t^{\text{em}}$  rather than total  $E_t$ . One sees a rise in planarity for  $E_t^{\text{em}}$  values above 6 GeV. A similar trend has already been reported by an ISR experiment.<sup>5</sup> A significant rise in the average planarity value is also observed as a function of  $E_t^{\text{had}}$  [Fig. (22(b))]. This is the first time that such a rise has been seen as a function of hadronic transverse energy.

We have checked this result by studying how the average planarity varies as a function of transverse energy deposited in the electromagnetic calorimeter modules (rather than using calorimeter tracks). A similar effect is seen and we conclude that the effect is not introduced by the algorithm that forms and separates electromagnetic and hadronic tracks.

In an attempt to understand the origin of the effect we have divided events with a given total  $E_t$  into three categories: those with a dominant fraction of electromagnetic energy ( $E_t^{\text{em}}/E_t > 0.6$ ), those with a dominant hadronic energy ( $E_t^{\text{had}}/E_t > 0.8$ ), and the remaining events ( $0.2 < E_t^{\text{em}}/E_t < 0.6$ ). The fraction of events with  $E_t^{\text{em}}/E_t > 0.6$  ( $E_t^{\text{had}}/E_t > 0.8$ ) increases with  $E_t^{\text{em}}$  ( $E_t^{\text{had}}$ ), as expected from simple kinematic constraints. Therefore we might expect the increase of  $\langle P \rangle$  with  $E_t^{\text{em}}$  or  $E_t^{\text{had}}$  observed in Fig. 22, to reflect the difference between mean planarities for events with large and medium values of the ratio  $E_t^{\text{em}}/E_t$  ( $E_t^{\text{had}}/E_t$ ), respectively.

In Fig. 23 we plot average planarity as a function of total  $E_t$  for the three categories of events. Indeed at all values of  $E_t$  events dominated by one type of energy have larger values of average planarity than the more balanced events. The difference between the average planarities for the two data sets is constant as a function of  $E_t$  up to  $E_t = 17$  GeV and only then starts to increase.

Events dominated by the one type of energy are characterized by smaller total particle multiplicities than the remaining events. This fact is consistent with the positive correlation between charged- and neutral-pion multiplicities<sup>27</sup> known from low- $p_t$  physics. However, it is not clear to what extent the observed correlation between  $\langle P \rangle$  and the ratio  $E_t^{\text{em}}/E_t$  ( $E_t^{\text{had}}/E_t$ ) reflects correlations between planarity and particle multiplicity discussed in the previous section. The LPS model fails to predict an increase of

$\langle P \rangle$  with  $E_t^{\text{em}}$  or  $E_t^{\text{had}}$ . The model correctly reproduces the difference between  $\langle P \rangle$  for balanced and unbalanced events up to  $E_t \leq 10$  GeV, but contrary to the data, predicts the difference to disappear with  $E_t$ .

We have also calculated two additional values of the planarity variable for each event using electromagnetic and hadronic tracks separately and studied their dependence on the corresponding type of transverse energy. The increase of average planarities of a given type at large transverse energies was found to be statistically insignificant.

#### F. $E_t$ cut on secondaries

The increase in planarity observed in events that were restricted to limited acceptances (in  $\phi$  or  $\theta^*$ ) is suggestive of a reduction of a possible source of "soft" background. This could also be the explanation of the increased planarity for constant multiplicity events. To investigate this further we have attempted to minimize the effect of low- $p_t$  secondaries by imposing the requirement  $p_t > 0.5$  GeV/ $c$  on all calorimeter tracks. No increase in average planarity was observable for high- $E_t$  events; in fact, little change occurred in the event structure when such a cut was applied.

There is also no indication of an increase with  $E_t$  in the fraction of total  $E_t$  carried by the most energetic or two most energetic calorimeter tracks (not shown). An increase of this type has been observed at higher energies.<sup>4-7</sup> This may be due to the "clusters" used in Refs. 4-7; they corresponded in size to jets rather than to single particles as in the case in our analysis.

From the studies described in this section we conclude that the data show a strong indication for the emergence of jetlike event structure even at the low-incident momentum of 400 GeV/ $c$ . Several different cuts on the data (restricting the azimuth of polar-angle acceptance of the apparatus, limiting the particle multiplicity, dividing events into electromagnetic and hadronic portions) produce effects that cannot be described by an extrapolation of uncorrelated low- $p_t$  phenomena. We interpret this as evidence for the onset of jet production ( $E_t > 14$  GeV).

## VII. PROPERTIES OF PLANAR EVENTS

In order to study the properties of events with planarity values greater than 0.7, we formed several variables using the transverse momenta associated with the calorimeter tracks.

First, we formed for each hadronic calorimeter track the variable  $x_p = 2E_t^{\text{had}}/E_t$ , where  $E_t^{\text{had}}$  was the transverse energy of the track and  $E_t$  was the total energy detected in the calorimeter. From Fig. 24, we see that the  $x_p$  distribution for low- and high-planarity events differ considerably. In Fig. 24(c) a comparison is made with the scaled hadron energy spectrum from  $e^+e^-$  annihilations at 14 GeV center-of-mass energy.<sup>28</sup> One can see that the high-planarity events from this experiment resemble the two-jet events produced in  $e^+e^-$  collisions. The E557 data do lie systematically below the  $e^+e^-$  distributions by almost a factor of 2, but this is probably due to the calorimeter

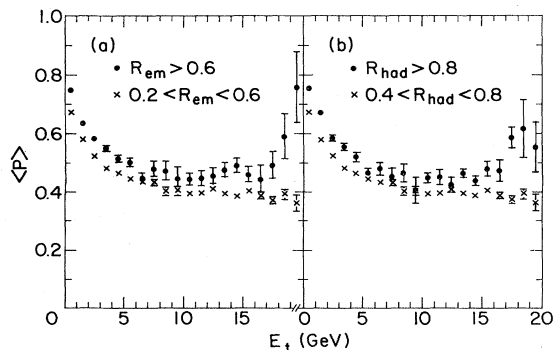


FIG. 23. Average planarity for events with relatively high values (circles) and medium values (crosses) of (a) electromagnetic and (b) hadronic transverse energy as a function of the total transverse energy in the calorimeter.

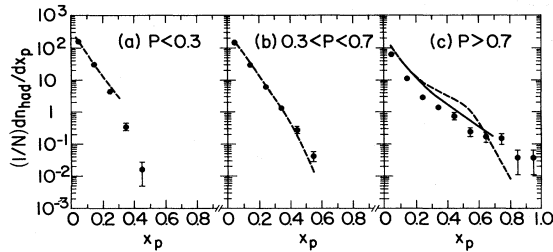


FIG. 24. Scaled transverse-energy distributions for hadronic tracks from high-transverse-energy events ( $E_t > 14$  GeV) with (a) low, (b) medium, and (c) high values of planarity. The solid curve in (c) is  $e^+e^-$  data (see Ref. 28); the dashed curve is the prediction of the QCD model. Only statistical errors are shown. Systematic uncertainties are estimated at  $\pm 20\%$ .

registering only a fraction of the away-side jet, contrary to the  $e^+e^-$  situation, where both jets are recorded (one can see this effect in the transverse-energy-flow plots, e.g., Fig. 14). Therefore the  $x_p$  distributions from this experiment are expected to have lower multiplicities.

The QCD model correctly reproduces the changes in the character of the distribution with increasing planarity, but overestimates the density of energetic particles of  $P > 0.7$  [see Fig. 24(c)].

In Fig. 25 we show how high-planarity ( $P > 0.7$ ) events change in structure as  $E_t$  is increased. At low  $E_t$  ( $E_t < 7$  GeV) the  $x_p$  distribution is strongly affected by single particles ( $x_p = 1$ ); from  $E_t = 7$  to 20 GeV only a small change in structure occurs. The slight “softening” of the distribution is in agreement with data from a previous experiment.<sup>10</sup>

We have investigated the jet structure within an event by dividing the event into two halves in the transverse plane. To do this an axis perpendicular to the planarity axis was used. Then, vector sums of the calorimeter-tracks momenta were formed. The directions of these sums formed, by definition, the two jet directions. The distribution of the projection of calorimeter-tracks momenta onto the jet direction was very similar to the  $x_p$  distributions. The distribution of the tracks momenta perpendicular to the jet direction is shown in Fig. 26. It can be seen that the high-planarity events are more collimated, as expected. One can see that “jets” from this experiment appear to be somewhat wider than those seen in 14-GeV center-of-mass energy  $e^+e^-$  collisions.<sup>29</sup>

### VIII. SUMMARY

We have presented results from an experiment which studied the production of high-transverse-energy events in  $pp$  collisions at a center-of-mass energy of 27.4 GeV. Only a small fraction of events ( $\sim 10\%$ ) exhibit jetlike structure. We have estimated that approximately half of those events are caused by dynamical effects other than statistical fluctuations of large-multiplicity low- $p_t$  events.

We have imposed several different restrictions on the data in order to select an unbiased sample of events with jetlike structure. Many of the cuts, e.g., restricting the az-

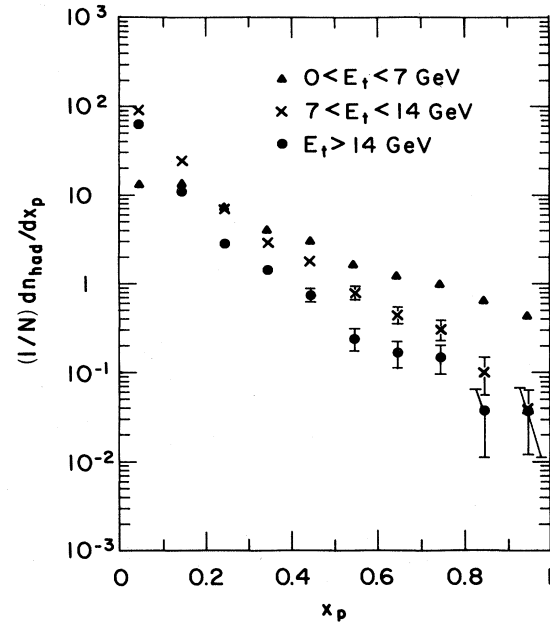


FIG. 25. Scaled transverse-energy distributions for hadronic tracks from high-planarity ( $P > 0.7$ ) events. Distributions for events with  $E_t < 7$  GeV (triangles),  $7 < E_t < 14$  GeV (crosses), and  $E_t > 14$  GeV (circles). Only statistical errors are shown.

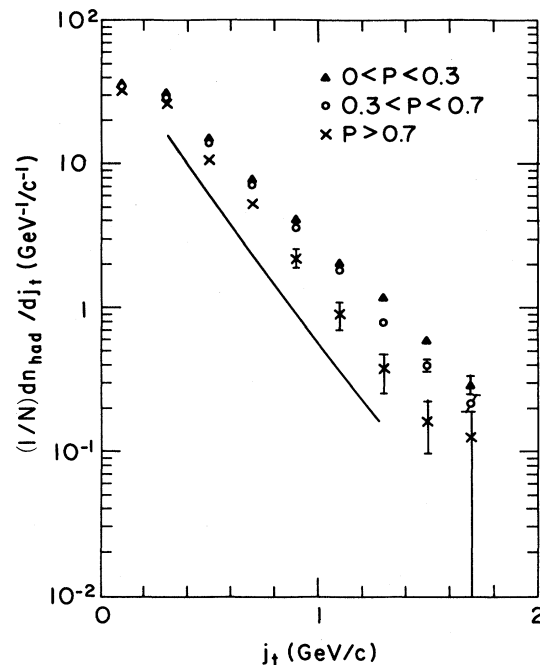


FIG. 26. Distributions of the component of hadronic track momenta perpendicular to the “jet” direction. Data from low- ( $P < 0.3$ ), medium- ( $0.3 < P < 0.7$ ), and high- ( $P > 0.7$ ) planarity events are shown. Data are for events with  $E_t > 14$  GeV. The solid curve is  $e^+e^-$  data (see Ref. 29).

imuth or polar-angle acceptance of the apparatus, limiting particle multiplicity, dividing events into electromagnetic and hadronic portions, produce effects that cannot be described by an extrapolation of uncorrelated low- $p_t$  phenomena. On the other hand, many aspects of the data agree qualitatively with the predictions of the QCD-gluon bremsstrahlung model. We conclude therefore that the data show an indication for the emergence of jetlike event structure even at the incident momentum of 400 GeV/ $c$ . However, due to the large background, a more quantitative separation of jet signal remains very model dependent.

#### ACKNOWLEDGMENTS

We are grateful for the excellent technical support given to us by the multiparticle-spectrometer-facility group led by Dan Green and by all the technical shops situated in the institutions that participated in this experiment. This work was supported in part by the U.S. Department of Energy and the National Science Foundation.

\*Present address: Higher Institute for Chemistry and Technology, Sofia, Bulgaria.

† Present address: Florida State University, Tallahassee, FL 32306.

‡ On leave of absence from University of Warsaw, Warsaw, Poland.

§ Present address: George Mason University, Fairfax, VA 22030.

<sup>1</sup>B. Brown *et al.*, Phys. Rev. Lett. **49**, 711 (1982).

<sup>2</sup>C. De Marzo *et al.*, Phys. Lett. **112B**, 173 (1982); Nucl. Phys. **B211**, 375 (1983).

<sup>3</sup>M. Arenton *et al.*, in *Proceedings of the 21st International Conference on High Energy Physics, Paris, 1982*, edited by P. Petiau and M. Porneuf [J. Phys. (Paris) Colloq. **43**, C3-131 (1982)].

<sup>4</sup>T. Akesson *et al.*, Phys. Lett. **128B**, 354 (1983).

<sup>5</sup>A. L. S. Angelis *et al.*, Phys. Lett. **126B**, 132 (1983).

<sup>6</sup>M. Banner *et al.*, Phys. Lett. **118B**, 203 (1982).

<sup>7</sup>G. Arnison *et al.*, Phys. Lett. **123B**, 115 (1983).

<sup>8</sup>G. C. Fox and R. L. Kelly, LBL-Caltech Report Nos. LBL-13985, CALT-68-890, 1982 (unpublished); R. D. Field, G. C. Fox, and R. L. Kelly, Phys. Lett. **119B**, 439 (1982).

<sup>9</sup>B. Brown *et al.*, Phys. Rev. Lett. **50**, 11 (1983).

<sup>10</sup>C. Bromberg *et al.*, Nucl. Phys. **B171**, 1 (1980).

<sup>11</sup>P. Rapp *et al.*, Nucl. Instrum. Methods **188**, 285 (1981).

<sup>12</sup>M. della Negra, Phys. Scr. **23**, 465 (1981).

<sup>13</sup>F. E. Taylor *et al.*, Phys. Rev. D **14**, 1217 (1976).

<sup>14</sup>D. Antreasyan *et al.*, Phys. Rev. D **19**, 764 (1979).

<sup>15</sup>H. Gordon *et al.*, Phys. Rev. D **28**, 2736 (1983).

<sup>16</sup>T. Akesson and H. U. Bengtsson, Phys. Lett. **120B**, 233 (1983).

<sup>17</sup>R. Singer *et al.*, Phys. Rev. D **25**, 2451 (1981).

<sup>18</sup>R. Odorico, Phys. Lett. **118B**, 151 (1982); Nucl. Phys. **B228**, 381 (1983).

<sup>19</sup>M. Greco, Phys. Lett. **121B**, 360 (1983).

<sup>20</sup>F. Bopp and P. Aurenche, Z. Phys. C **13**, 205 (1982).

<sup>21</sup>C. Halliwell, in *Multiparticle Dynamics, 1982*, proceedings of the XIIIth International Symposium, Volendam, The Netherlands, edited by W. Kittel, W. Metzger, and A. Stergiou (World Scientific, Singapore, 1983), p. 509.

<sup>22</sup>T. L. Watts, in *Proceedings of the 21st International Conference on High Energy Physics, Paris, 1982* (Ref. 3) [J. Phys. (Paris) Colloq. **43**, C3-127 (1982)].

<sup>23</sup>C. Bromberg *et al.*, Phys. Rev. Lett. **31**, 1563 (1973); Nucl. Phys. **B107**, 82 (1976).

<sup>24</sup>R. P. Feynman, R. D. Field, and G. C. Fox, Phys. Rev. D **18**, 3320 (1978).

<sup>25</sup>R. D. Field and R. P. Feynman, Nucl. Phys. **B136**, 1 (1978).

<sup>26</sup>T. Akesson *et al.*, Phys. Lett. **118B**, 185 (1982); **123B**, 133 (1983).

<sup>27</sup>R. D. Kass *et al.*, Phys. Rev. D **20**, 605 (1976).

<sup>28</sup>R. Brandelik *et al.*, Phys. Lett. **114B**, 65 (1982).

<sup>29</sup>R. Brandelik *et al.*, Phys. Lett. **86B**, 243 (1979).